Received: 24 July 2020 | Revised: 26 October 2020 | Accepted: 30 October 2020

DOI: 10.1002/bmc.5020

RESEARCH ARTICLE

Biomedical Chromatography WILEY

The related mechanism of complete Freund's adjuvant-induced chronic inflammation pain based on metabolomics analysis

Weibo Zhang[1] | Jie Lyu[1] | Juxiang Xu[3] | Piao Zhang[1] | Shuxia Zhang[1] | Yeru Chen[1] | Yongjie Wang[2] | Gang Chen[1]

[1]Department of Anesthesiology, Sir Run Run Shaw Hospital, School of Medicine, Zhejiang University, Zhejiang, Hangzhou, China

[2]Institute of Neuroscience and Collaborative Innovation Center for Brain Science, School of Medicine, Zhejiang University, Zhejiang, Hangzhou, China

[3]Department of Radiotherapy Nursing Unit, Sir Run Run Shaw Hospital, School of Medicine Zhejiang University, Hangzhou, China

Correspondence
Gang Chen, Department of Anesthesiology, Sir Run Run Shaw Hospital, School of Medicine, Zhejiang University, 3 Qingchun East Road. Hangzhou, Zhejiang 310016, China.
Email: chengang120@zju.edu.cn

Funding information
Key Program of the Natural Science Foundation of Zhejiang Province, China, Grant/Award Number: No. LZ19H090003; National Natural Science Foundation of China, Grant/Award Number: No.81371214 and No.81671063; Natural Science Foundation of Zhejiang Province, China, Grant/Award Number: No.LY16H090008

Abstract

Chronic inflammation pain is a debilitating disease, and its mechanism still remains poorly understood. This study attempted to illuminate the metabolic mechanism of chronic inflammation pain induced by complete Freund's adjuvant (CFA) injection, especially at spinal level. The chronic inflammation pain model was established by CFA administration. Behavioral testing including mechanical allodynia and thermal hyperalgesia was performed. Meanwhile, a liquid chromatography–mass spectrometry-based metabolomics approach was applied to analyze potential metabolic biomarkers. The orthogonal partial least squares discrimination analysis mode was employed for determining metabolic changes, and a western blot was performed to detect the protein expression change. The results showed that 27 metabolites showed obviously abnormal expression and seven metabolic pathways were significantly enriched, comprising aminoacyl-tRNA biosynthesis, arginine and proline metabolism, histidine metabolism, purine metabolism, phenylalanine, tyrosine and tryptophan biosynthesis, glutathione metabolism, and phenylalanine metabolism. Meanwhile, the results showed that the expression of arginase I and nitric oxide levels were elevated in the CFA group compared with the control group, while the argininosuccinate synthetase and argininosuccinatelyase proteins were not significantly different between the groups. These findings demonstrate that metabolic changes of the spinal cord may be implicated in neurotransmitter release and pain conductivity following CFA administration.

KEYWORDS
chronic inflammation pain, complete Freund's adjuvant, metabolomics

1 | INTRODUCTION

Chronic pain results in dramatic decline in life quality, substantial medical expenses and a massive economic burden (Henderson & Keay, 2018). Survey data demonstrate that the prevalence of chronic pain ranges from 13.5 to 47% globally, and afflicts at least 50 million American adults (Dahlhamer et al., 2018; Tsuji et al., 2019). Generally, patients with chronic pain have symptoms of anxiety and depression, poor concentration and irritability (Gureje, Von Korff, Simon, & Gater, 1998). Some research shows that patients with chronic pain have multiple inflammatory and neuropathic conditions (Finnerup, 2013). Additionally, chronic inflammation pain, as one type

of chronic pain, is attracting growing interest from clinicians and scientists. A previous study documented that chronic inflammation pain was derived from chemical stimuli, tissue damage or autoimmune processes. These stimuli directly caused the release of inflammatory mediators comprising prostaglandins, histamine and neurogenic factors, and elicited a series of chain reactions, thereby contributing to pain sensation by stimulating the peripheral afferent fibers (Kidd, Photiou, & Inglis, 2004). The potential mechanism regarding the chronic inflammation pain has been extensively investigated. Yet, it is of great importance in the clinical practice, while its pathogenesis has not been clarified comprehensively.

More recently, systems biology strategies such as metabolomics have been widely applied in medical fields to investigate the pathogenic mechanism, which facilitated the development of novel biomarkers for disease diagnosis and therapy (Hocher & Adamski, 2017; Yang et al., 2018; Zhang et al., 2018). Metabolism is a complex dynamic process including generating energy and producing macromolecules for sustaining cell growth and survival (Patti et al., 2012). Metabolites are downstream molecules of gene transcription and translation processes, which are closely correlated to the disease phenotype (Lains et al., 2019). Metabolic shift is identified as a hallmark of disease, and provides a noninvasive method to monitor the disease progress (Ohman & Forsgren, 2015). Furthermore, emerging evidence has revealed the relationship between inflammatory and metabolic dysregulation (Jha et al., 2015; Jiang et al., 2016; Palomer, Salvado, Barroso, & Vazquez-Carrera, 2013). A previous study revealed that aberrant metabolism may be involved in triggering inflammatory cascade reactions (O'Neill & Hardie, 2013). Notwithstanding, there are no adequate data to uncover the role of metabolism alteration in chronic inflammation pain. Therefore, the complete Freund's adjuvant (CFA) model was established to investigate the potential mechanism for chronic inflammation pain in this study. Moreover, a metabolomics method was employed to analyze the changes in spinal metabolites. Interestingly, our results indicated that certain metabolic pathways were obviously enriched in the chronic inflammatory process, and these findings may provide new perspectives for comprehending the underlying mechanism of chronic inflammation pain.

2 | MATERIALS AND METHODS

2.1 | Animals

All experiments were performed on 8–12-week-old male C57BL/6 mice purchased from Shanghai SLAC Laboratory Animal Co. Ltd. For experiments, mice (20–35 g) were housed four or five per cage at constant room temperature (25 ± 1°C) and relative humidity (50 ± 5%) under a 12 h light/dark schedule (lights on 07:00–19:00); food and water were available *ad libitum*. For behavioral tests, the mice were allowed to adapt to laboratory conditions for about one week and to habituate to the testing situation for at least 15 min before experiments. The Animal Care and Use Committee of Zhejiang University approved all of the mouse protocols (approval no. 11978).

2.2 | CFA-induced chronic inflammation pain

Animals were randomly divided into two groups as follows: (a) a control group, injected with 10 μl saline (n = 10); and (b) a CFA group, injected with 10 μl 50% CFA in saline (n = 10). Chronic inflammatory pain was induced by administration of CFA as described previously (Pan et al., 2014). Briefly, an emulsion containing 10 μl of CFA with saline (proportion 1:1) was injected into the left posterior plantar of mice (n = 10). The control group received the same procedure with saline (Y. Liu et al., 2017b). Mice were allowed to acclimatize to the home cage and environment.

2.3 | Behavioral testing

2.3.1 | Mechanical allodynia

Mice were placed in individual black wood boxes without a bottom and allowed to acclimatize for at least 30 min to quantify the mechanical sensitivity of the hindpaw according to the previous literature (Chaplan, Bach, Pogrel, Chung, & Yaksh, 1994). Mechanical paw withdrawal threshold in response to the stimulation of von Frey filaments was measured using the "up–down" method (Chaplan, Bach, Pogrel, Chung, & Yaksh, 1994). Filaments were applied to the plantar surface of left hindpaw until they bent. A quick withdrawal or shaking of the stimulated paw or biting or licking of the paw was regarded as a positive withdrawal response, while other responses were regarded as a negative withdrawal response. A positive withdrawal response was followed by the application of a lower force filament and vice versa for a negative response until a change in behavior occurred (Zhao, Hiraoka, Ogawa, & Tanaka, 2018). The test started with the application of a 0.16 g filament. Every trial was repeated three times at ~2 min intervals. According to the method described by Dixon, the 50% paw withdrawal threshold was calculated based on this assessment.

2.3.2 | Thermal hyperalgesia

To assess thermal hyperalgesia, mouse paw withdrawal latency (PWL) was measured using radiant heat (Bao et al., 2014; Bao et al., 2015). Mice were placed individually in plastic cages and allowed to acclimatize at least for 30 min. Each left hind paw received at least three stimuli with a 10 min interval between, and the average of the three values was defined as the PWL. The heat was maintained at a constant intensity and the cut-off time was set to 21 s to prevent paw damage.

2.3.3 | Sample preparation

Animals were anesthetized with 3% isoflurane on day 7 after CFA administration. Then these mice were sacrificed through decapitation. A laminectomy of L4–6 was carried out, and the spinal cord tissues

were exposed. Complete incision of L4–6 was performed and the intervening tissue was removed. Thereafter, the spinal cord was removed and stored in a liquid nitrogen box immediately for future use.

2.3.4 | Metabolite extraction

In brief, the spinal cord tissue was homogenized in 1,500 μl methanol with water (1:1) in a 2 ml glass tissue homogenizer, and centrifuged at 15,000***g*** for 10 min (Tube 1). The supernatant was transferred to a 2 ml centrifuge tube, tube 2, then concentrated at room temperature in vacuum. A 120 μl methanol–water (1:1) solution was applied to dissolve the concentrated product. The precipitate of tube 1 was homogenized with 1,600 μl cold dichloromethane–methanol (3:1), then centrifuged at 15,000***g*** for 10 min. The culture liquid was transferred to 2 ml centrifuge tube, tube 3, which was concentrated at room temperature in vacuum, and redissolved with 120 μl methanol–water (1:1). The solutions of centrifuge tubes 2 and 3 were mixed and centrifuged once again (15,000***g*** for 10 min). The supernatant was determined by HPLC–MS. During the study, 10 QC samples were pooled from all spinal cord samples to equilibrate the HPLC–MS system (Zhou et al., 2018).

2.3.5 | Liquid chromatography–mass spectrometry analysis

The metabolomics data were determined using a Nexera UHPLC LC-30A system (Shimadzu, Japan), while the chromatographic separation was processed on a Waters HSS T3 (150 × 3 mm, 1.8 μm) column at 25°C, with a flow rate of 0.3 ml/min. The analysis was completed with mobile phases A (acetonitrile) and B (0.1% CH_3COOH–H_2O). The gradient program was 100% B at 0–10 min; 50% A and 50% B at 10–13 min; 95% A and 5% B at 13–14 min; 100% B at 14–15 min. All samples were kept at 4°C during the procedures.

The high-resolution MS system was performed using a TripleTOF5600 + mass spectrometer (AB SCIEX™, USA). Both positive and negative modes was used to acquire the data. Source parameters are defined as follows: scanning range, *m/z* 100–1,500; scanning mode,data-independent acquisition (DIA); capillary voltage, 5,000 V (positive) and 4,500 V (negative); capillary temperature, 500°C; declustering potential (DP), 60 V; collision energy (CE), 35 V; collision energy spared (CES), 15 V.

2.3.6 | Data processing

The raw LC–MS data was imported into MS-DIAL3.96 software for preprocessing, then peak extraction, de-noise, deconvolution and peak alignment, and a 3D data matrix in CSV format was exported. The peak information was compared with metabolites from online databases including MassBank, Respect and GNPS. The three-dimensional matrix comprising sample information, retention time, mass nuclear ratio and mass spectrometry response intensity (peak area) was analyzed. Principal components analysis, partial least squares discriminate analysis and orthogonal partial least squares discrimination analysis were carried out to make multivariate statistical analysis using SIMCA-P (version 11.0, Umetrics, Umea, Sweden) software (Rezig et al., 2018).

2.3.7 | Western blot analysis

The mouse spinal cord tissues (L4–6) were harvested and homogenized using RIPA buffer (Beyotime, P0013B) supplemented with 1× protease inhibitor cocktail (Sigma-Aldrich; P8304), phosphatase inhibitor cocktail II and III (Sigma-Aldrich; P5726). The supernatant was collected by centrifugation at 12,000***g*** for 10 min, and the protein concentration was detected using a bicinchoninic acid protein assay kit (Beyotime, P0012S). An aliquot of 50 μg protein from each sample was separated using SDS-PAGE and transferred to a PVDF membrane, then blocked with 5% nonfat milk in TBST (pH 7.4). Thereafter, the membranes were incubated with primary antibodies including arginase I (1:1000; CST; #93668), argininosuccinate synthetase (1:1000; abcam; ab17095), argininosuccinatelyase (1:1000; abcam; ab97370) and actin (1:1000; ABclonal; AC026). After incubation with the appropriate horseradish peroxidase (HRP) conjugated secondary antibodies (IgG, against rabbit, 1:1000; ABclonal; AS014), the immune complexes were visualized using the SuperSignal West Pico Substrate (34,077, Pierce). The digital images were quantified using densitometric measurements by Quantity-One software (Bio-Rad).

2.3.8 | NO level detection

The spinal cord tissues (L4–6) were acquired and the level of nitric oxide (NO) was determined. Briefly, the NO detection kit (A012-1-2; Nanjing Jiancheng Biotechnology Co. Ltd; China) was purchased and the experiment protocol was performed according to the operating manual.

2.3.9 | Statistical analysis

Data are presented as the mean ±standard deviation. An unpaired Student's *t*-test was conducted using GraphPad Prism 8.0 (Graphpad, CA, USA). A value of $P < 0.05$ was considered statistically significant.

3 | RESULTS

3.1 | CFA-induced mechanical and thermal hypersensitivities

The mechanical and thermal hypersensitivities were examined on the fifth day after CFA injection. The results showed that the PWL and

paw withdrawal threshold values were remarkable decreased in the CFA group compared with the control group (Figure 1a,b; $P < 0.05$).

3.2 | Metabolic profiling analysis

To confirm whether chronic inflammation pain induced dramatic shifts in the metabolites in the spinal cord, an LC–MS method was applied to analyze the differences between the control and CFA groups. Principal components analysis (Figure 2a) and partial least squares discrimination analysis methods (Figure 2b) were used to detect the differences. The results showed that the two methods did not isolate differentially expressed metabolites (Figure 2a,b). Therefore, orthogonal partial least squares discrimination analysis mode was employed, and the metabolites were separated into two categories (Figure 2c). Meanwhile, the model was subjected to a parametric test, and the results indicated that the prediction rate of metabolites was 14.4%, the prediction rate of the grouping was 75.4% and the accuracy of model prediction was 58.6% (Figure 2d). In order to prevent a false positive of the model, it was detected by response arrangement tests (100 runs), and the results showed that the prediction rate of grouping was 99.0%, and the accuracy of model prediction was 72.3% (Figure 2e). To obtain different metabolite candidates, *P*-value < 0.05 and fold change > 2 were set as threshold values. The heat map and volcano plot of metabolites are separately shown in Figure 2f and g, and the details of the different metabolites are attached to Table 1.

3.3 | Protein expression and pathway analysis

The decrease in arginine levels may be involved in the alteration of key enzymes of the arginine–NO cycle including argininosuccinate synthetase and argininosuccinatelyase, and NO level and arginase I expression. To validate the hypothesis, the Western Blot (WB) assay was performed, and the results showed that the expression of arginase I was elevated in the CFA group compared with the control group, while the proteins of argininosuccinate synthetase and argininosuccinatelyase were not significantly different between the CFA group and the control group (Figure 3a). The NO level was obviously increased in the CFA group compared with the control group (Figure 3b, $P < 0.05$). In order to screen significantly enriched pathways, the different metabolites were analyzed based on the KEGG and HMDB databases. In Table 2, metabolic pathways with raw *P* and impact values are listed. In addition, the impact of metabolic pathway is delineated in Figure 3c, and the pathways marked with letters were severely affected by chronic inflammation pain, with the details as follows (A–G): (A) aminoacyl-tRNA biosynthesis; (B) arginine and proline metabolism; (C) histidine metabolism; (D) purine metabolism; (E) phenylalanine; (F) tyrosine and tryptophan biosynthesis; and (G) glutathione metabolism and phenylalanine metabolism. Moreover, to provide insight into the pathobiological mechanism of chronic inflammation pain, the interaction networks among these seven metabolic pathways were generated and are presented in Figure 3d.

4 | DISCUSSION

Chronic inflammatory pain is universally regarded as a difficult medical problem worldwide and only partial therapy options are available. Various methods have been employed to investigate the potential mechanisma. However, the complex biochemical processes of chronic inflammatory pain remain poorly understood and little relief has been achieved in spite of the enormous efforts that have been made in basic medical and clinical research. Therefore, illuminating the underlying mechanism may provide novel strategies to alleviate pain with fewer side effects. Recently, systems biology strategies including metabolomics analysis have been widely applied to explore the pathogenic mechanism. In this study, the metabolites of CFA-induced chronic inflammation pain were analyzed based on a metabolomics method. The analysis showed that 27 metabolites were significantly altered in response to CFA injection and seven metabolic pathways were obviously enriched.

4.1 | The association between chronic inflammatory pain and metabolites

Inflammatory pain is a complex symptom involving multiple modulators consisting of neurotransmitters, receptors, ion channels and signaling pathways (Jiao et al., 2020). Previous studies documented that NF-κB, as a ubiquitously expressed transcription factor, could effectively initiate the inflammatory response to mediate

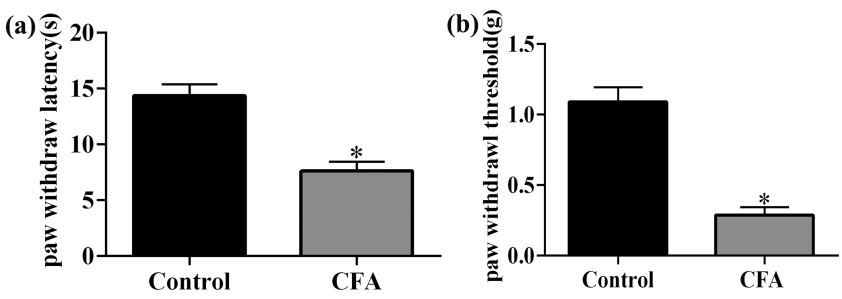

FIGURE 1 Mechanical and thermal allodynia in mice induced by complete Freund's adjuvant (CFA) injection. Effect of CFA injection on the paw withdrawal responses to thermal (a) and mechanical (b) stimuli at 5 days. *$P < 0.05$, compared with control group

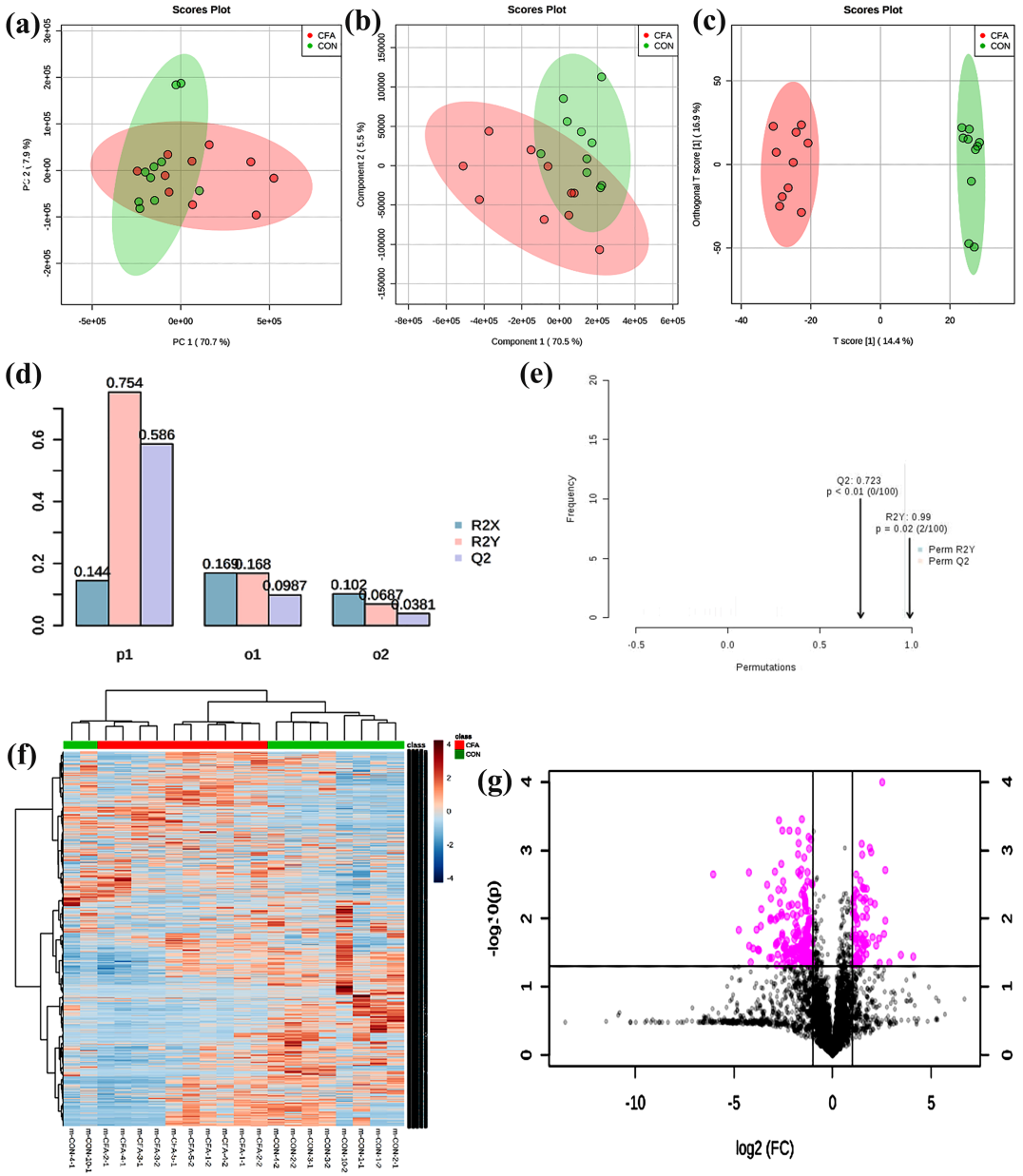

FIGURE 2 Metabolic profiling analysis: (a) principal components analysis; (b) partial least squares discrimination analysis; (c) orthogonal partial least squares discrimination analysis; (d, e) parametric test. (f) Heat map analysis of metabolites between control group and CFA group (the color scale shows the relative metabolites expression in certain slide: blue indicates low relative expression levels; red indicates high relative expression levels; yellow indicates no change); (g) volcano plot of metabolites between control group and CFA group (red indicates the metabolites expression was significantly down/up-regulated in CFA group compared with control group; $P < 0.05$). R^2X represents the prediction rate of metabolites, R^2Y represents the prediction rate of grouping, and Q^2 represents the accuracy of model prediction

cell proliferation, apoptosis and metastasis (Sethi, Sung, & Aggarwal, 2008). Insulin resistance was enhanced by the NF-κB pathway to accelerate the progress of inflammatory reactions (Wang, Zhang, Wang, Wang, & Liu, 2019). Inflammatory and oxidative stress were closely correlated with the development of metabolic complications, and NF-κB signaling may promote the deterioration of non-alcoholic fatty liver disease by inducing the accumulation of triacylglycerol in the liver (Kang et al., 2017; Valenzuela & Videla, 2020). Moreover, emerging evidence has shown that metabolic disturbance may participate in regulating excitable membranes, synaptic transmission and synaptic plasticity. Surveys suggested several metabolites as biological markers that are sensitive to pain pathology induced by CFA injection. Similarly, the differentially expressed metabolites were screened, and the results showed that the expression of 26 metabolites was significantly changed in response to CFA injection. Hence, the potential regulatory network was analyzed, and a hub metabolite was sought out for developing a therapeutic method of chronic inflammation pain.

TABLE 1 The details of metabolites in different groups

Alignment ID	Average retention time (min)	Average Mz	Metabolite name	Adduct type	MS/MS assigned	Reference *m/z*	Formula	Ontology
44	3.798	104.05289	*N*-Methylalanine	$[M + H]^+$	True	104.0706	$C_4H_9NO_2$	Alanine and derivatives
47	2.967	104.07158	a-Aminoisobutyrate	$[M + H]^+$	True	104.0706	$C_4H_9NO_2$	Alpha amino acids
634	3.507	132.101	Isoleucine	$[M + H]^+$	True	132.1028	$C_6H_{13}NO_2$	Isoleucine and derivatives
1,006	4.964	146.16362	Spermidine	$[M + H]^+$	True	146.16518	$C_7H_{19}N_3$	Dialkylamines
1,093	3.779	150.05882	Methionine	$[M + H]^+$	True	150.05832	$C_5H_{11}NO_2S$	Methionine and derivatives
1,149	4.075	156.0755	Histidine	$[M + H]^+$	True	156.07675	$C_6H_9N_3O_2$	Histidine and derivatives
1,254	3.967	161.12683	L-β-Homolysine	$[M + H]^+$	True	161.12845	$C_7H_{16}N_2O_2$	β Amino acids and derivatives
1,285	3.391	162.11143	L-carnitine	$[M + H]^+$	True	162.11247	$C_7H_{15}NO_3$	Carnitines
1,291	3.753	162.112	Carnitine	$[M + H]^+$	True	162.11247	$C_7H_{15}NO_3$	Carnitines
1,572	3.702	182.08066	Tyrosine	$[M + H]^+$	True	182.08118	$C_9H_{11}NO_3$	Tyrosine and derivatives
2,218	1.391	220.11549	D-(+)-pantothenic acid	$[M + H]^+$	True	220.11795	$C_9H_{17}NO_5$	Secondary alcohols
2,298	4.286	227.11293	L-Carnosine	$[M + H]^+$	True	227.11386	$C_9H_{14}N_4O_3$	Hybrid peptides
2,657	1.416	245.07281	Uridine	$[M + H]^+$	True	245.07681	$C_9H_{12}N_2O_6$	Pyrimidine nucleosides
2,948	6.998	261.03534	D-Mannose-6 -phosphate	$[M + H]^+$	True	261.03699	$C_6H_{13}O_9P$	Hexose phosphates
3,133	2.362	269.08701	Inosine	$[M + H]^+$	True	269.08804	$C_{10}H_{12}N_4O_5$	Purine nucleosides
4,947	6.973	364.06473	Guanosine 5′-monophosphate	$[M + H]^+$	True	364.06528	$C_{10}H_{14}N_5O_8P$	Purine ribonucleoside monophosphates
55	1.398	115.00401	Maleic acid	$[M - H]^-$	True	115.00368	$C_4H_4O_4$	Dicarboxylic acids and derivatives
217	3.937	154.06157	His	$[M - H]^-$	True	154.06219	$C_6H_9N_3O_2$	Histidine and derivatives
263	3.67	164.07458	L-(−)-Phenylalanine	$[M - H]^-$	True	164.0717	$C_9H_{11}NO_2$	Phenylalanine and derivatives
301	6.907	171.00775	Glycerophosphate(2)	$[M - H]^-$	True	171.00639	$C_3H_9O_6P$	Glycerophosphates
312	1.694	173.00899	*cis*-Aconitate	$[M - H]^-$	True	173.00916	$C_6H_6O_6$	Tricarboxylic acids and derivatives
317	4.026	173.10483	L-(+)-Arginine	$[M - H]^-$	True	173.1044	$C_6H_{14}N_4O_2$	L-α-Amino acids
803	6.769	229.0134	D-Ribulose 5-phosphate	$[M - H]^-$	True	229.01187	$C_5H_{11}O_8P$	Pentose phosphates
1718	5.74	322.0506	Cytidine-3′ -monophosphate	$[M - H]^-$	True	322.04459	$C_9H_{14}N_3O_8P$	Ribonucleoside 3′-phosphates
1731	6.877	323.02869	Uridine 5′ -monophosphate	$[M - H]^-$	True	323.02859	$C_9H_{13}N_2O_9P$	Pyrimidine ribonucleoside monophosphates

TABLE 1 (Continued)

Alignment ID	Average retention time (min)	Average Mz	Metabolite name	Adduct type	MS/MS assigned	Reference *m/z*	Formula	Ontology
3,024	7.264	476.09399	8-Methylthiooctyl glucosinolate	$[M-H]^-$	True	476.10883	$C_{16}H_{31}NO_9S_3$	Alkylglucosinolates

TABLE 1 (Continued)

Alignment ID	INCHIKEY	SMILES	MS1 isotopic spectrum	MS/MS spectrum	m-CON-1-1	m-CON-1-2	m-CON-2-1	m-CON-2-2
					CON	CON	CON	CON
44	GDFAOVXKHJXLEI-VKHMYHEASA-N	CN[C@@H](C)C(O)=O	104.05318:10556 105.05653:4518 106.05989:904	58.07356:42104.11706:42	2,194	813	6,113	23,888
47	FUOOLUPWFVMBKG-UHFFFAOYSA-N	CC(C)(N)C(O)=O	104.06766:5184 105.07101:4230 106.07437:2256	56.05714:83 58.07238:2343 58.11862:142 58.14444:98 58.21546:42 58.37488:42 59.05377:43 59.08196:319 59.1004:63 59.91335:48 60.08711:1660 60.11774:104 60.19324:42 60.48803:42 61.00925:63 69.03474:42 71.08587:42 87.05281:63104. 10562:1224 104.28419:42	62,703	54,945	78,732	42,530
634	AGPKZVBTJJNPAG-UHFFFAOYNA-N	O=C(O)C(N)C(C)cc	132.101:275158 133.10435:40078 134.10771:5289	53.00695:63 53.02544:42 55.02148:42 55.06335:83 56.06026:171 57.06399:150 57.07038:149 58.05942:83 58.0691:63 58.07985:63 62.94052:21 69.04636:63 69.07684:478 69.10146:102 69.21879:42 71.07623:42 72.06087:146 72.08722:42 72.94139:146 73.06555:63 74.0699:42 85.8249:42 86.09304:87 86.1022:2372 86.20303:179 86.27247:83 86.34325:83 86.53212:42 87.06313:210 87.08025:133 87.09867:104 89.60625:44 90.05688:982 90.90903:42 114.07255:63115.05105:6 3117.0801:42119.07763:21 127.86925:43132.07666: 840132.11559:42	14,260	715	869	106,976

TABLE 1 (Continued)

Alignment ID	INCHIKEY	SMILES	MS1 isotopic spectrum	MS/MS spectrum	m-CON-1-1	m-CON-1-2	m-CON-2-1	m-CON-2-2
1,006	ATHGHQPFGPMSJY-UHFFFAOYSA-N	NCCCCNCCCN	146.16512:4739 147.16847:688 148.17183:0	56.96902:21 58.07324:42 72.08226:146 72.09304:104 84.08359:63112.11149:42	53	69	1,045	3,522
1,093	FFEARJCKVFRZRR-UHFFFAOYNA-N	CSCCC(N)C(O)=O	150.056:51970 151.05935:5422 152.06271:8131	53.04919:42 53.06153:42 55.87885:31 56.05933:1175 56.10476:77 56.12907:45 58.99855:42 60.82431:42 60.85072:48 61.01922:1374 61.07874:47 61.54713:21 66.04822:31 70.9967:21 73.64085:21 74.02877:191 74.05183:31 74.06519:73 75.03236:31 77.00658:31 84.04641:83 84.05804:63 85.03094:83 87.0238:53 87.02644:234 90.04098:31 93.06465:21102.05724:190 104.05369:350105.00134:3 1120.0837:21129.12486:10 133.03197:514134.11136:4 2135.12294:31150.05905:8 3150.07806:42150.12646:52	991	2,193	3,376	7,331
1,149	HNDVDQJCIGZPNO-UHFFFAOYNA-N	O=C(O)C(N)CC1=CN=CN1	156.07379:27948 157.07714:3718 158.0805:3718	50.02816:21 54.04945:63 56.06555:147 66.04694:83 68.05582:83 71.95312:42 81.04317:42 81.04952:169 82.05473:167 82.07135:63 83.05714:44 83.06357:331 83.10729:42 86.06815:21 93.04813:366 95.05525:22 95.06213:63109.721:65110 .07299:883110.1026:6911 1.05206:42115.50999:211 56.07678:83	2,559	3,836	10,967	5,033
1,254	PJDINCOFOROBQW-LURJTMIESA-N	NCCCC[C@H](N)CC(O)=O	161.12852:5683 162.13187:1610 163.13523:1610	70.07452:21 72.08102:125 8 4.08356:83 84.10168:6313 9.03064:21144.10316:63146 .07782:42161.1118:42	4,751	1,240	3,089	56,286

TABLE 1 (Continued)

Alignment ID	INCHIKEY	SMILES	MS1 isotopic spectrum	MS/MS spectrum	m-CON-1-1	m-CON-1-2	m-CON-2-1	m-CON-2-2
1,285	PHIQHXFUZVPYII-ZCFIWIBFSA-N	C[N+](C)(C)C[C@H](O)CC([O-])=O	162.11374:29728 163.11709:5364 164.12045:1490	57.03634:42 58.07023:104 59.07545:63 60.09476:104 85.03355:104102.09293:104103.03878:104103.04737:146146.09703:63162.11127:503	137,818	126,043	189,429	120,297
1,291	PHIQHXFUZVPYII-ZCFIWIBFSA-N	C[N+](C)(C)C[C@H](O)CC([O-])=O	162.11185:524328 163.1152:89133 164.11856:11269	54.93892:42 55.95581:43 57.04489:618 57.06727:96 57.09925:54 58.07563:878 59.07764:378 59.35122:63 60.01388:48 60.08713:1754 60.11119:177 60.12213:95 60.13635:111 61.0302:125 61.06437:42 84.08521:42 84.76316:63 85.03355:2327 85.0882:99 86.05917:42 97.97429:42 98.96687:421 02.09148:1763 103.04305:2444 103.08173:102103.22644:83104.41814:42114.96052:42146.10208:63161.58708:83162.10399:264162.11296:4560 162.25131:661 62.34656:125162.44545:104	114,299	2,126,919	2,391,938	55,919
1,572	OUYCCCASQSFEME-UHFFFAOYNA-N	O=C(O)C(N)CC1=CC=C(O)C=C1	182.08034:80922 183.08369:11783 184.08705:2561	51.03576:63 53.04057:148 53.06729:42 55.02642:31 64.8437:32 65.04722:246 67.05714:42 74.79868:21 77.0445:333 77.07794:36 79.05739:73 79.08247:21 81.03526:21 81.06955:52 88.02511:21 90.77292:42 91.05811:2809 91.10388:61 91.16583:43 93.05737:31 94.04394:42 94.75534:52 95.05221:776 95.08797:26 95.10586:26 99.93855:2110 1.04308:31103.05828:941 06.06608:22107.05055:50 1108.08651:21109.06851: 52117.05843:83118.06648: 167118.66663:42119.0511 6:1528 119.09734:34120.0 5537:31121.0638:83122.64	8,060	623	884	226,568

(Continues)

TABLE 1 (Continued)

Alignment ID	INCHIKEY	SMILES	MS1 isotopic spectrum	MS/MS spectrum	m-CON-1-1	m-CON-1-2	m-CON-2-1	m-CON-2-2
				606:21123.04481:1296 123 .37523:21135.06503: 31135.66908:32136.075 27:2217 137.07275:42145. 26024:21147.04427:41515 3.06671:32165.05525:4581 82.07918:52				
2,218	GHOKWGTUZJEAQD -ZETCQYMHSA-N	CC(C)(CO)[C@@H] (O)C(O)=NC CC(O)=O	220.11549:34997 221.11884:3891 222.1222:1196	56.01493:42 57.07793:63 59.06138:42 67.06334:83 69.08517:42 70.03354:63 72.04784:63 77.04002:42 79.05535:42 83.05476:42 85.06741:63 87.08044:42 90.05307:85 90.05977:337 94.07184:42 95.05688:83 98.01903:42 98.02183:831 15.06196:42118.09472:631 22.10828:21124.07578:14 6129.08815:42131.08987: 42142.08527:104145.099 5:42156.11259:42177.1265 4:104184.09784:125202.10 573:104202.14784:21205.1 2944:63205.1638:167205.1 7592:104220.11571:12522 0.14291:42	210,166	167,154	220,827	109,474
2,298	CQOVPNPJLQNMDC -ZETCQYMHSA-N	NCCC(O)=N[C@@H] (CC1=CN=CN1)C(O)=O	227.1124:74781 228.11575:11134 229.11911:1465	55.04132:42 68.05227:42 82 .05465:63 83.06734:215 83 .08278:64 84.96175:42 93. 0494:146 93.84448:43 95.0 634:235109.72236:47 110.07436:1878 110.1069 2:69110.16467:57119.075 93:63122.07659:361122.0 875:147136.08853:63141. 10925:21146.08275:63151 .03488:21152.08218:83155 .33369:43156.07483:71216 1.68329:21164.07979:23017 2.06091:21180.08009:6318 1.10577:125192.07181:422 10.0862:188210.1046:1042 24.81111:21227.10995:104 227.12697:83	18,611	8,659	3,375	691,174

TABLE 1 (Continued)

Alignment ID	INCHIKEY	SMILES	MS1 isotopic spectrum	MS/MS spectrum	m-CON-1-1	m-CON-1-2	m-CON-2-1	m-CON-2-2
2,657	DRTQHJPVMGBUCF-UHFFFAOYNA-N	O=C1N=C(O)C=CN1C2OC(co)C(O)C2O	245.07242:3838 246.07577:45224 7.07913:0	70.02979:42 71.02264:21 96.01913:63 97.0379:4211 3.02923:65113.03673:5371 13.06073:42245.22159:63	69,991	42,498	24,696	39,146
2,948	NBSCHQHZLSJFNQ-QTVWNMPRSA-N	OC1O[C@H](COP(O)(O)=O)[C@@H](O)[C@H](O)[C@@H]1O	261.03534:50962 262.03869:4518 263.04205:1061	53.04903:63 57.04477:63 63.03564:21 67.02851:21 69.03809:106 71.04882:42 80.98725:85 81.03551:281 85.03593:230 93.06441:21 97.04065:43 98.98625:426 99.02415:71 99.04521:149100.90723:42103.3968:44109.03044:725109.09969:23118.94981:21127.04094:383127.05207:127145.04797:63160.98993:21207.00189:42225.00177:42225.01447:104243.02344:146	62,030	31,393	42,363	123,232
3,133	UGQMRVRMYYASKQ-KQYNXXCUSA-N	OC[C@H]1O[C@H]([C@H](O)[C@@H]1O)N1C=NC2=C1N=CN=C2O	269.08591:112501 270.08926:17870 271.09262:3310	55.02217:63 55.03473:42 57.04338:83 57.06256:63 67.03049:42 69.03893:63 71.02114:63 73.03501:83 82.05434:83 85.02518:42 85.03168:63 85.04599:63 92.02988:42 94.03973:213 95.21723:21 97.02918:42 99.83833:42103.04815:43 110.03708:674115.04003:85118.6619:43119.03718:769120.0197:104133.04759:83136.60722:209137.04619:23885 137.17505:1682 137.26263:667137.3519:250137.39655:42137.48917:42137.55205:167137.64471:125137.81856:125138.30925:63138.40051:42140.32079:42215.12384:42219.2112:21	1,744,192	2,301,859	1,189,128	1,606,597
4,947	RQFCJASXJCIDSX-UUOKFMHZSA-N	O[C@@H]1[C@@H](COP(O)(O)=O)O[C@H]([C@@H]1O)N1C=NC2=C1NC(=N)N=C2O	364.05899:1155 365.06234:434366.0657:87	110.05524:10135.02759:21149.02536:21152.05627:125152.08411:631	683	2,643	263	6,031

(Continues)

TABLE 1 (Continued)

Alignment ID	INCHIKEY	SMILES	MS1 isotopic spectrum	MS/MS spectrum	m-CON-1-1	m-CON-1-2	m-CON-2-1	m-CON-2-2
				69.94139:10264.2 6987:10				
55	VZCYOOQTPOCHFL -UHFFFAOYSA-N	O=C(O)C=cc(=O)O	115.00503:9050 116.00838:577 117.01174:576	71.05444:21 71.05563:21	55,633	77,348	48,858	62,670
217	HNDVDQJCIGZPNO -YFKPBYRVSA-N	N[C@@H](CC1=CN=C N1)C(O)=O	154.06317:5394 155.06652:6751 56.06988:630	80.04959:42 91.03069:21 9 3.0517:83137.04097:4 2154.07217:63	2,130	584	2,731	2,805
263	COLNVLDHVKWLRT -QMMMGPOBSA-N	N[C@@H](CC1=CC= CC=C1)C(O)=O	164.07387:12947 165.07722:2343 166.08058:1340	72.01447:42 91.05745:2110 3.06355:42134.04286:211 47.05013:104164.08469:63	59,723	1,231	4,593	37,941
301	AWUCVROLDVIAJX -GSVOUGTGSA-N	OC[C@@H](O)COP(O) (O)=O	171.01015:13672 172.0135:624173. 01686:286	77.99744:43 78.96368:57 9 81.30538:21	193,915	455,002	195,998	313,002
312	GTZCVFVGUGFEME -IWQZZHSRSA-N	OC(=O)C\C(=C\C(O)= O)C(O)=O	173.01173:4774 174. 01508:988175.018 44:188	85.03636:63	26,885	37,094	29,617	1902
317	ODKSFYDXXFIFQN -BYPYZUCNSA-N	N[C@@H](CCCNC(N)= N)C(O)=O	173.10464:16345 174.10799:2098 175.11135:74	105.03072:21131.0858:37 8173.11749:42	9,483	93,266	131,938	8,595
803	FNZLKVNUWIIPSJ -UHNVWZDZSA-N	OCC(=O)[C@H](O)[C@H] (O)COP(O)(O)=O	229.00995:5537 230.0133:849231 .01666:282	78.95767:63 78.96269:294 91.06715:21 96.97551:125 97.03944:42	59,792	54,366	146,915	51,521
1718	UOOOPKANIPLQPU -XVFCMESISA-N	OC[C@H]1O[C@H]([C@H] (O)[C@@H]1OP(O)(O)=O) N1C=CC(=N)N=C1O	322.0498:4108 323. 05315:759324.0 5651:333	78.96099:125 96.97363:422 11.01308:42322.06519:63	33,820	128,567	23,557	160,602
1731	DJJCXFVJDGTHFX -XVFCMESISA-N	O[C@@H]1[C@@H](COP (O)(O)=O)O[C@H]([C@ @H]1O)N1C=CC(O)=N C1=O	323.03195:4429 324.0353:820325. 03866:412	78.96327:167 80.51807:21 96. 97334:83111.02354:42 211.00215:63323.03467:63	29,233	149,656	17,963	202,163
3,024	CWOJBEDMJKZKAB -STPBKMPXSA-N	CSCCCCCCCC\C(S[C@@ H]1O[C@H](CO)[C@@H] (O)[C@H](O)[C@H]1O) =N/OS(O)(=O)=O	476.0961:3018 477 .09945:479478. 10281:695	96.98495:42357.10968:42 389.07697:104458.1270 1:21476.10638:167476.127 93:188	33,371	34,322	19,035	24,637

TABLE 1 (Continued)

Alignment ID	m-CON-3-1	m-CON-3-2	m-CON-4-1	m-CON-4-2	m-CON-5-1	m-CON-5-2	m-CFA-1-1	m-CFA-1-2
	CON	CON	CON	CON	CON	CON	CFA	CFA
44	45,403	29,632	46,466	46,437	50,186	6,318	52,019	38,489
47	87,202	80,753	98,610	104,309	96,175	82,126	91,306	110,792
634	120,636	816	154,014	34,887	3,356	859	15,242	1,267
1,006	8,376	7,891	12,487	8,258	28,946	582	12,503	25,642
1,093	5,339	1925	248,496	8,429	224,333	1867	12,403	9,580
1,149	9,758	57,934	130,906	8,141	45,796	2,921	167,330	124,687
1,254	40,507	44,075	15,866	60,653	13,569	372	77,838	74,484
1,285	182,996	226,630	171,583	230,633	230,463	1,617	354,025	440,909
1,291	39,264	15,737	7,897	45,777	2049	2,570,282	27,836	16,605
1,572	388,549	282,080	350,601	507,047	346,685	2	433,140	282,783
2,218	147,563	108,886	56,756	58,130	89,778	218,550	133,007	121,659
2,298	7,229	672,318	676,762	765,788	534,700	11,967	994,556	706,764
2,657	37,751	48,829	31,960	31,420	14,001	31,382	9,996	37,357
2,948	220,245	70,522	88,688	424,738	442,372	825,961	540,513	331,605
3,133	1,083,286	1,455,366	1,113,897	1,444,050	899,913	1,494,445	1,074,040	1,458,989
4,947	1,126	1,516	323	5,970	5,029	4,968	1877	7,575
55	32,151	49,493	32,421	69,355	21,203	39,650	26,928	50,276
217	1,596	25,392	32,088	2,772	46,927	1924	37,518	31,430
263	77,746	57,819	75,580	88,057	81,639	137	100,927	61,536
301	258,938	165,165	293,164	184,300	291,288	304,236	128,549	153,126
312	1,439	1,126	1,095	1,447	1725	52,483	1791	2,320
317	20,461	7,508	6,163	15,823	9,093	60,177	10,077	6,734
803	86,127	4,758	31,327	69,766	35,181	109,452	14,016	7,827
1718	21,139	14,234	34,175	26,041	13,700	33,224	10,321	34,112
1731	18,277	21,042	29,042	20,533	14,499	28,719	13,747	23,658
3,024	14,148	28,477	7,809	21,548	27,341	22,910	13,362	10,208

TABLE 1 (Continued)

Alignment ID	m-CFA-2-1	m-CFA-2-2	m-CFA-3-1	m-CFA-3-2	m-CFA-4-1	m-CFA-4-2	m-CFA-5-1	m-CFA-5-2
	CFA	CFA	CFA	CFA	CFA	CFA	CFA	CFA
44	45,164	35,816	72,491	40,667	48,518	38,682	43,410	72,211
47	92,627	107,516	125,306	114,844	154,416	108,947	156,350	139,787
634	1,462,686	8,721	1,404,377	1,314,712	1,672,418	3,525	1,578	6,252
1,006	29,045	21,045	21,998	26,846	70,867	113,281	56,294	62,733
1,093	203,402	208,821	281,816	185,274	234,987	262,779	342,045	404,916
1,149	40,716	143,928	67,014	47,851	26,308	44,872	318,432	290,404
1,254	15,263	81,451	31,709	26,618	22,144	20,078	22,976	94,105
1,285	1,259,888	305,598	292,446	335,317	1,768,962	338,206	430,799	398,995
1,291	9,793	17,451	1,601	9,851	14,734	10,385	11,670	23,891
1,572	263,639	318,859	309,281	265,574	326,698	310,226	493,607	582,405
2,218	44,553	87,255	76,023	81,978	30,429	92,765	114,592	121,395
2,298	307,627	838,688	664,714	681,011	67,650	941,312	717,540	803,866
2,657	14,007	17,556	2,538	28,768	2,617	11,325	1824	1,048
2,948	354,822	396,896	424,848	373,235	413,106	497,578	948,371	689,780
3,133	656,759	1,296,131	533,352	1,233,329	494,316	966,957	696,056	1,027,346
4,947	1,051	9,004	11,751	1790	17,554	11,665	7,104	8,026
55	11,637	51,514	32,987	25,449	20,385	39,037	39,291	29,654
217	44,829	28,002	50,461	38,582	49,224	31,520	50,570	2,223
263	6,396	65,599	92,867	78,271	85,666	57,850	103,083	116,152
301	10,999	162,820	9,070	9,053	9,921	189,087	256,611	127,301
312	682	1,536	1,215	1,062	1,274	1,506	2057	2,623
317	1,693	9,333	6,493	6,422	4,270	7,258	14,847	34,069
803	28,820	11,103	33,714	42,339	35,598	68,688	61,508	9,504
1718	10,600	21,033	19,820	12,858	16,402	12,454	13,615	9,089
1731	1,557	17,368	1978	2031	2,303	20,274	14,242	5,319
3,024	10,621	9,090	6,317	19,145	6,381	14,649	9,622	6,535

TABLE 1 (Continued)

Alignment ID	QC-1	QC-2	QC-3	QC-4	QC-5			
	QC	QC	QC	QC	QC	VIP (CFA vs. CON)	FC (CFA vs. CON)	TTEST (CFA vs. CON)
44	3,369	2,412	35,398	1967	37,982	0.060775	1.8934433871	0.0041166709
47	20,239	3,645	41,971	67,113	61,782	0.10933	1.5250778787	0.0002315302
634	49,284	40,378	42,667	43,929	38,667	1.4409	13.4680832579	0.017904852
1,006	741	71	346	63	856	0.097503	6.1808252257	0.0010790023
1,093	410	4,593	2,204	824	219,231	0.43378	4.2556179107	0.0022510742
1,149	3,874	2,741	3,303	6,566	4,009	0.26255	4.5763448755	0.0061254643
1,254	3,417	867	2,832	2,743	7,909	0.059781	1.9411417257	0.0421885982
1,285	1,008	1,020	117,255	123,861	125,978	1.1382	3.6631295405	0.007597821
1,291	2,141,254	2,090,007	104,083	166,766	41,578	1.9093	0.0195136254	0.0288782904
1,572	230	1,033	343,879	8,427	382,659	0.38975	1.6987417454	0.0247046305
2,218	95,250	291,906	285,777	247,110	218,772	0.12778	0.6513850084	0.0240294256
2,298	459	802	451,869	13,045	501,460	0.88068	1.9830595505	0.0156686685
2,657	30,913	36,493	47,935	42,544	40,265	0.064638	0.3417941529	0.0004340064
2,948	426	6,442	11,014	48,095	52,117	0.69733	2.1319580501	0.0090084967
3,133	1,380,913	1,675,873	1,554,619	1,649,054	1,345,126	1.2935	0.6584421129	0.0042157925
4,947	49	129	273	28	443	#N/A	2.710738302	0.007436557
55	45,173	36,089	41,432	43,091	38,137	0.042704	0.6693331587	0.0155992248
217	1,664	3,377	1898	4,881	3,229	0.064842	3.063153116	0.0012762611
263	59,012	58,157	61,426	63,599	64,054	0.075006	1.5859668171	0.0361989234
301	125,714	155,695	163,806	208,021	204,086	0.42234	0.3979411738	0.0003830492
312	24,108	19,080	22,670	20,288	20,534	#N/A	0.1037768146	0.0177163028
317	17,284	17,708	8,559	20,185	9,741	0.069043	0.2791559887	0.0419059935
803	38,938	49,583	50,449	52,324	56,902	0.0888	0.4823083618	0.0170326847
1718	29,710	32,516	39,322	35,315	39,940	0.086863	0.3277804927	0.0305979778
1731	34,845	38,533	36,869	43,415	47,390	0.11326	0.1929425542	0.0284777076
3,024	9,484	13,047	20,190	11,853	19,247	0.033732	0.4534713482	0.0001821421

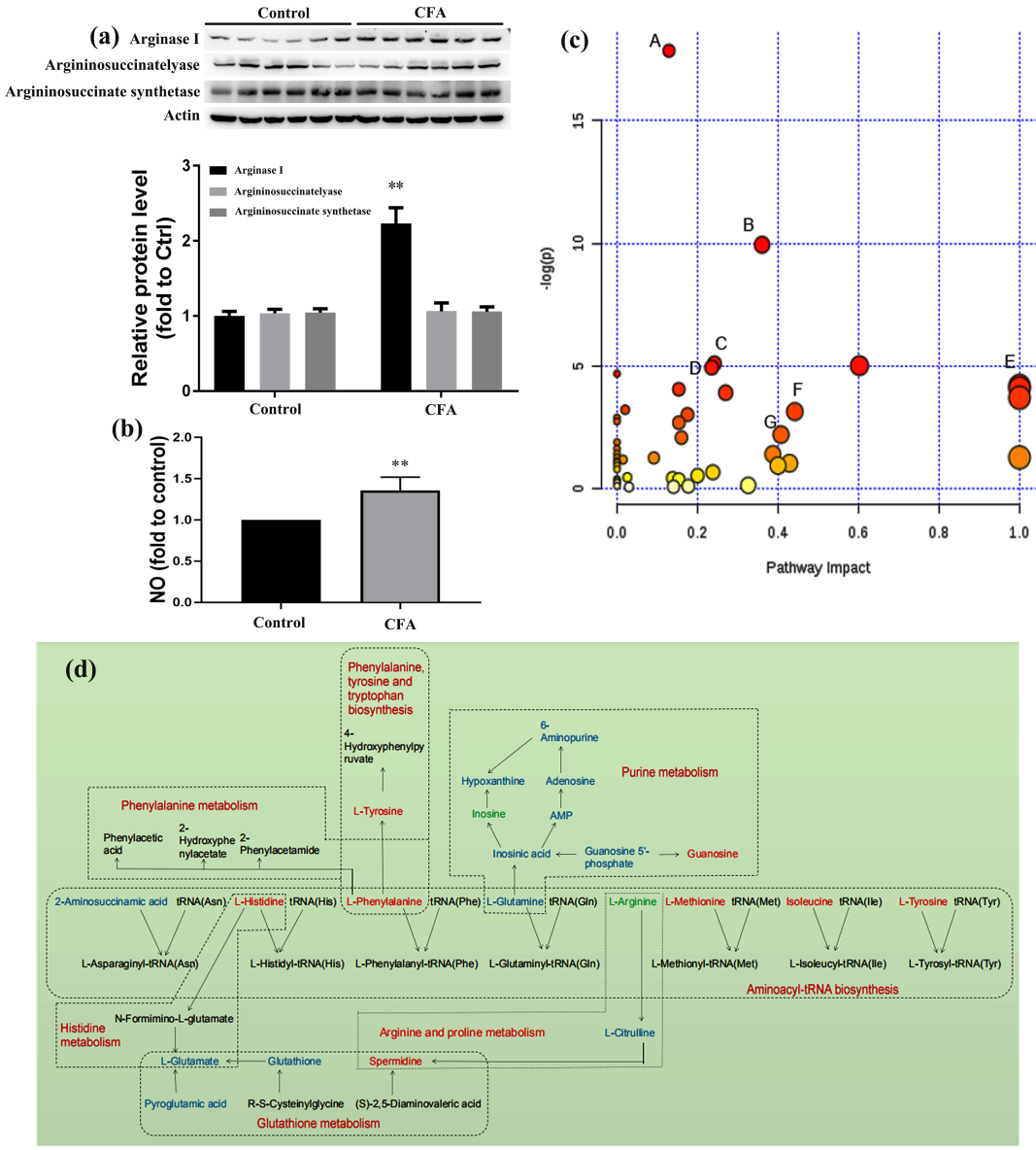

FIGURE 3 Pathway analysis of the different metabolites: (a) Western Blot (WB) assay for key protein expression; (b) NO level detection; and (c) bubble plot for pathway analysis of the different metabolites. The *x*-axis represents the pathway impact and the *y*-axis describes the impact value. The circular area is proportional to the number of metabolites assigned to the term and the color accords with the *P*-value; (d) the regulatory relationship of metabolic pathways in response to CFA-induced inflammatory pain. Potential biomarkers are marked as red (up-regulated), green (down-regulated) and blue (without significant changes). Other undetected metabolites in the metabolic pathway are labeled in black. The names of related metabolic pathways are marked in red in the corresponding dashed box

4.2 | The metabolic alterations elicited by chronic inflammatory pain

Several metabolites induced by chronic inflammatory pain were identified, which may be implicated in nervous impulse transmission. To clarify the metabolic process, spinal cord tissues were acquired and the regulatory process of metabolites was analyzed. Generally, arginine is susceptible to the level of guanidine compounds, and thereby results in citrullination (Wang et al., 2019). In addition, a previous study showed that arginine downregulation exacerbated the inflammatory reactions, and thereby resulted in the degradation of amino acids (Schroecksnadel et al., 2006). In this study, our results showed that the level of arginine was significantly decreased in the CFA group compared with the control group, which may directly mediate the inflammatory response and cause inflammatory pain. In addition, related documents revealed that arginine participated in the synthesis of NO neurotransmitter, which could produce anti-nociceptive natural opioids and *N*-methyl-D-aspartate receptor-mediated pain-promoting effect (Chen et al., 2016; Rondon et al., 2018), whereas neurotransmitter depletion derived from arginine decrease may contribute to inflammatory pain. Moreover, histidine is closely related to the inflammation processes by regulating the synthesis of histamine

TABLE 2 The potential metabolic pathways

	Total	Expected	Hits	Raw *P*	#name?	Holm adjust	FDR	Impact
Aminoacyl-tRNA biosynthesis	69	3.6034	17	1.81×10^{-8}	17.827	1.48E-06	1.48E-06	0.12903
Arginine and proline metabolism	44	2.2978	10	4.84×10^{-5}	9.9365	0.0039184	0.0019834	0.36034
Histidine metabolism	15	0.78335	4	0.0060344	5.1103	0.48275	0.11698	0.24194
Alanine, aspartate and glutamate metabolism	24	1.2534	5	0.0066071	5.0196	0.52196	0.11698	0.60232
Purine metabolism	68	3.5512	9	0.0071327	4.9431	0.55635	0.11698	0.23524
Nitrogen metabolism	9	0.47001	3	0.0091513	4.6939	0.70465	0.12507	0
Phenylalanine, tyrosine and tryptophan biosynthesis	4	0.20889	2	0.015078	4.1945	1	0.15742	1
Valine, leucine and isoleucine biosynthesis	11	0.57445	3	0.016665	4.0944	1	0.15742	0.99999
Pyrimidine metabolism	41	2.1411	6	0.017278	4.0583	1	0.15742	0.1534
Glycine, serine and threonine metabolism	31	1.6189	5	0.019841	3.92	1	0.1627	0.26989
D-Glutamine and D-glutamate metabolism	5	0.26112	2	0.024285	3.7179	1	0.18103	1
Pantothenate and CoA biosynthesis	15	0.78335	3	0.039543	3.2304	1	0.26972	0.02041
Glutathione metabolism	26	1.3578	4	0.04276	3.1522	1	0.26972	0.44179
Cysteine and methionine metabolism	27	1.41	4	0.048266	3.031	1	0.2827	0.17491
β-Alanine metabolism	17	0.88779	3	0.054848	2.9032	1	0.29984	0
Biosynthesis of unsaturated fatty acids	42	2.1934	5	0.063642	2.7545	1	0.32333	0
Glycerophospholipid metabolism	30	1.5667	4	0.067032	2.7026	1	0.32333	0.15371
Phenylalanine metabolism	11	0.57445	2	0.10909	2.2156	1	0.49694	0.40741
Amino sugar and nucleotide sugar metabolism	37	1.9323	4	0.12318	2.0941	1	0.53164	0.16012
Ubiquinone and other terpenoid–quinone biosynthesis	3	0.15667	1	0.14873	1.9056	1	0.60979	0
Lysine biosynthesis	4	0.20889	1	0.19328	1.6436	1	0.75471	0
Biotin metabolism	5	0.26112	1	0.23553	1.4459	1	0.86	0
Glyoxylate and dicarboxylate metabolism	18	0.94001	2	0.24122	1.4221	1	0.86	0.38709
Cyanoamino acid metabolism	6	0.31334	1	0.27559	1.2888	1	0.886	0
Linoleic acid metabolism	6	0.31334	1	0.27559	1.2888	1	0.886	1
Citrate cycle (TCA cycle)	20	1.0445	2	0.28093	1.2697	1	0.886	0.09164
Sphingolipid metabolism	21	1.0967	2	0.30076	1.2014	1	0.91341	0.01504
Valine, leucine and isoleucine degradation	38	1.9845	3	0.31867	1.1436	1	0.93324	0
Lysine degradation	23	1.2011	2	0.34013	1.0784	1	0.9556	0
Taurine and hypotaurine metabolism	8	0.41778	1	0.34961	1.0509	1	0.9556	0.42857
Ascorbate and aldarate metabolism	9	0.47001	1	0.38377	0.95772	1	0.9834	0
Methane metabolism	9	0.47001	1	0.38377	0.95772	1	0.9834	0.4
Riboflavin metabolism	11	0.57445	1	0.44686	0.80551	1	1	0
Nicotinate and nicotinamide metabolism	13	0.6789	1	0.50357	0.68603	1	1	0.2381
Pentose and glucuronate interconversions	16	0.83557	1	0.57805	0.54809	1	1	0.2
Glycerolipid metabolism	18	0.94001	1	0.62147	0.47567	1	1	0.0256
Starch and sucrose metabolism	19	0.99224	1	0.64149	0.44396	1	1	0.13815
Fatty acid biosynthesis	43	2.2456	2	0.6688	0.40227	1	1	0
Fructose and mannose metabolism	21	1.0967	1	0.67845	0.38794	1	1	0.15342
Butanoate metabolism	22	1.1489	1	0.6955	0.36313	1	1	0
Galactose metabolism	26	1.3578	1	0.7552	0.28077	1	1	0
Fatty acid elongation in mitochondria	27	1.41	1	0.76823	0.26367	1	1	0
Porphyrin and chlorophyll metabolism	27	1.41	1	0.76823	0.26367	1	1	0
Arachidonic acid metabolism	36	1.88	1	0.85855	0.15251	1	1	0.32601

(Continues)

TABLE 2 (Continued)

	Total	Expected	Hits	Raw *P*	#name?	Holm adjust	FDR	Impact
Fatty acid metabolism	39	2.0367	1	0.88011	0.12771	1	1	0
Tryptophan metabolism	40	2.0889	1	0.88655	0.12042	1	1	0.17715
Tyrosine metabolism	44	2.2978	1	0.90906	0.095343	1	1	0.14045
Primary bile acid biosynthesis	46	2.4023	1	0.9186	0.084902	1	1	0.02976

neurotransmitters (Shell et al., 2016). The metabolomics data showed that histidine expression was enhanced following CFA injection and ultimately led to chronic inflammation pain.

4.3 | Phenylalanine and tyrosine metabolism

Tyrosine is an essential amino acid, which is partially synthetized from phenylalanine. The accumulation of phenylpyruvate is toxic to the central nervous system (Rausell et al., 2019). Previous research found that the levels of phenylalanine and tyrosine were remarkably increased in cerebrospinal fluid of patients with regional pain syndrome (Meissner et al., 2014). Dopamine, norepinephrine and epinephrine produced by the phenylalanine and tyrosine metabolic reactions play a critical role in the brain. Norepinephrine released from the sympathetic nerves can activate β2ARs receptors, and result in production and secretion of the proinflammatory cytokine, subsequently causing hyperalgesia of sensory neurons and increasing chronic inflammatory pain (Li et al., 2013). Interestingly, our findings indicated that the pronounced increase of phenylalanine and tyrosine may accelerate pain signal transduction by increasing the concentration of neurotransmitters in spinal cord.

Currently, data suggest that metabolic changes are relevant to many diseases, and metabolites obtained from accessible samples such as urine or plasma may serve as potential biomarkers for diagnosis of chronic inflammatory pain in the clinic (Liu et al., 2017a; Liu et al., 2017b). The spinal cord is the primary center of transmission signals. The signals of nociceptive stimuli are transmitted to the posterior horn of the spinal cord by fine fibers, and eventually pass to the cerebral cortex after processing in the spinal cord (Descalzi et al., 2015; Meacham, Shepherd, Mohapatra, & Haroutounian, 2017).

Therefore, investigating the alteration of metabolites in spinal cord may help to illuminate the neuronal communication mechanism regarding CFA injection-induced chronic inflammation pain. Collectively, this study provides a new perspective for comprehending the pathological process of CFA-induced chronic inflammation pain, and enhancing efforts to develop new therapeutic strategies.

ACKNOWLEDGEMENTS

This study was supported by the National Natural Science Foundation of China (nos 81371214 and 81671063), the Natural Science Foundation of Zhejiang Province, China (no. LY16H090008), and the Key Program of the Natural Science Foundation of Zhejiang Province, China (no. LZ19H090003).

COMPETING INTERESTS

The authors declare that they have no competing interests.

ORCID

Gang Chen https://orcid.org/0000-0002-8359-7417

REFERENCES

Bao, Y., Gao, Y., Hou, W., Yang, L., Kong, X., Zheng, H., … Hua, B. (2015). Engagement of signaling pathways of protease-activated receptor 2 and mu-opioid receptor in bone cancer pain and morphine tolerance. *International Journal of Cancer*, *137*(6), 1475–1483. https://doi.org/10.1002/ijc.29497

Bao, Y., Hou, W., Liu, R., Gao, Y., Kong, X., Yang, L., … Hua, B. (2014). PAR2-mediated upregulation of BDNF contributes to central sensitization in bone cancer pain. *Molecular Pain*, *5*(10), 28.

Chaplan, S. R., Bach, F. W., Pogrel, J. W., Chung, J. M., & Yaksh, T. L. (1994). Quantitative assessment of tactile allodynia in the rat paw. *Journal of Neuroscience Methods*, *53*(1), 55–63.

Chen, G., Xie, R. G., Gao, Y. J., Xu, Z. Z., Zhao, L. X., Bang, S., … Ji, R. R. (2016). Beta-arrestin-2 regulates NMDA receptor function in spinal lamina II neurons and duration of persistent pain. *Nature Communications*, *7*, 12531. https://doi.org/10.1038/ncomms12531

Dahlhamer, J., Lucas, J., Zelaya, C., Nahin, R., Mackey, S., DeBar, L., … Helmick, C. (2018). Prevalence of chronic pain and high-impact chronic pain among adults—United States, 2016. *MMWR. Morbidity and Mortality Weekly Report*, *67*(36), 1001–1006. https://doi.org/10.15585/mmwr.mm6736a2

Descalzi, G., Ikegami, D., Ushijima, T., Nestler, E. J., Zachariou, V., & Narita, M. (2015). Epigenetic mechanisms of chronic pain. *Trends in Neurosciences*, *38*(4), 237–246. https://doi.org/10.1016/j.tins.2015.02.001

Finnerup, N. B. (2013). Pain in patients with spinal cord injury. *Pain*, *154* (Suppl 1), S71–S76. https://doi.org/10.1016/j.pain.2012.12.007

Gureje, O., Von Korff, M., Simon, G. E., & Gater, R. (1998). Persistent pain and well-being: A World Health Organization study in primary care. *JAMA*, *280*(2), 147–151. https://doi.org/10.1001/jama.280.2.147

Henderson, L. A., & Keay, K. A. (2018). Imaging acute and chronic pain in the human brainstem and spinal cord. *The Neuroscientist*, *24*(1), 84–96. https://doi.org/10.1177/1073858417703911

Hocher, B., & Adamski, J. (2017). Metabolomics for clinical use and research in chronic kidney disease. *Nature Reviews. Nephrology*, *13*(5), 269–284. https://doi.org/10.1038/nrneph.2017.30

Jha, M. K., Song, G. J., Lee, M. G., Jeoung, N. H., Go, Y., Harris, R. A., … Suk, K. (2015). Metabolic connection of inflammatory pain: Pivotal role of a pyruvate dehydrogenase kinase–pyruvate dehydrogenase–lactic acid axis. *The Journal of Neuroscience*, *35*(42), 14353–14369. https://doi.org/10.1523/JNEUROSCI.1910-15.2015

Jiang, H., Liu, J., Wang, T., Gao, J. R., Sun, Y., Huang, C. B., … Qin, X. J. (2016). Urinary metabolite profiling provides potential differentiation to explore the mechanisms of adjuvant-induced arthritis in rats.

Biomedical Chromatography, *30*(9), 1397–1405. https://doi.org/10.1002/bmc.3697

Jiao, Q., Ren, Y., Ariston Gabrie, A. N., Wang, Q., Wang, Y., Du, L., … Wang, Y. S. (2020). Advances of immune checkpoints in colorectal cancer treatment. *Biomedicine & Pharmacotherapy*, *123*, 109745. https://doi.org/10.1016/j.biopha.2019.109745

Kang, H. H., Kim, I. K., Lee, H. I., Joo, H., Lim, J. U., Lee, J., … Moon, H. S. (2017). Chronic intermittent hypoxia induces liver fibrosis in mice with diet-induced obesity via TLR4/MyD88/MAPK/NF-κB signaling pathways. *Biochemical and Biophysical Research Communications*, *490*(2), 349–355. https://doi.org/10.1016/j.bbrc.2017.06.047

Kidd, B. L., Photiou, A., & Inglis, J. J. (2004). The role of inflammatory mediators on nociception and pain in arthritis. *Novartis Foundation Symposium*, *260*, 122–133.discussion 133–128, 277–129

Lains, I., Gantner, M., Murinello, S., Lasky-Su, J. A., Miller, J. W., Friedlander, M., & Husain, D. (2019). Metabolomics in the study of retinal health and disease. *Progress in Retinal and Eye Research*, *69*, 57–79. https://doi.org/10.1016/j.preteyeres.2018.11.002

Li, W., Shi, X., Wang, L., Guo, T., Wei, T., Cheng, K., … Clark, J. D. (2013). Epidermal adrenergic signaling contributes to inflammation and pain sensitization in a rat model of complex regional pain syndrome. *Pain*, *154*(8), 1224–1236. https://doi.org/10.1016/j.pain.2013.03.033

Liu, R., Xu, H., Zhang, X., Wang, X., Yuan, Z., Sui, Z., … Li, Q. (2017a). Metabolomics strategy using high resolution mass spectrometry reveals novel biomarkers and pain-relief effect of traditional Chinese medicine prescription Wu-Zhu-Yu decoction acting on headache modelling rats. *Molecules*, *22*(12). https://doi.org/10.3390/molecules22122110

Liu, Y., Chen, H., Lu, J., Jiang, Y., Yang, R., Gao, S., … Chen, W. (2017b). Urinary metabolomics of complete Freund's adjuvant-induced hyperalgesia in rats. *Biomedical Chromatography*, *31*(6). https://doi.org/10.1002/bmc.3886

Meacham, K., Shepherd, A., Mohapatra, D. P., & Haroutounian, S. (2017). Neuropathic pain: Central vs. peripheral mechanisms. *Current Pain and Headache Reports*, *21*(6), 28. https://doi.org/10.1007/s11916-017-0629-5

Meissner, A., van der Plas, A. A., van Dasselaar, N. T., Deelder, A. M., van Hilten, J. J., & Mayboroda, O. A. (2014). ^{1}H-NMR metabolic profiling of cerebrospinal fluid in patients with complex regional pain syndrome-related dystonia. *Pain*, *155*(1), 190–196. https://doi.org/10.1016/j.pain.2013.10.005

Ohman, A., & Forsgren, L. (2015). NMR metabonomics of cerebrospinal fluid distinguishes between Parkinson's disease and controls. *Neuroscience Letters*, *594*, 36–39. https://doi.org/10.1016/j.neulet.2015.03.051

O'Neill, L. A., & Hardie, D. G. (2013). Metabolism of inflammation limited by AMPK and pseudo-starvation. *Nature*, *493*(7432), 346–355. https://doi.org/10.1038/nature11862

Palomer, X., Salvado, L., Barroso, E., & Vazquez-Carrera, M. (2013). An overview of the crosstalk between inflammatory processes and metabolic dysregulation during diabetic cardiomyopathy. *International Journal of Cardiology*, *168*(4), 3160–3172. https://doi.org/10.1016/j.ijcard.2013.07.150

Pan, Z., Zhu, L. J., Li, Y. Q., Hao, L. Y., Yin, C., Yang, J. X., … Cao, J. L. (2014). Epigenetic modification of spinal miR-219 expression regulates chronic inflammation pain by targeting CaMKIIgamma. *The Journal of Neuroscience*, *34*(29), 9476–9483. https://doi.org/10.1523/JNEUROSCI.5346-13.2014

Patti, G. J., Yanes, O., Shriver, L. P., Courade, J. P., Tautenhahn, R., Manchester, M., & Siuzdak, G. (2012). Metabolomics implicates altered sphingolipids in chronic pain of neuropathic origin. *Nature Chemical Biology*, *8*(3), 232–234. https://doi.org/10.1038/nchembio.767

Rausell, D., Garcia-Blanco, A., Correcher, P., Vitoria, I., Vento, M., & Chafer-Pericas, C. (2019). Newly validated biomarkers of brain damage may shed light into the role of oxidative stress in the pathophysiology of neurocognitive impairment in dietary restricted phenylketonuria patients. *Pediatric Research*, *85*(2), 242–250. https://doi.org/10.1038/s41390-018-0202-x

Rezig, L., Servadio, A., Torregrossa, L., Miccoli, P., Basolo, F., Shintu, L., & Caldarelli, S. (2018). Diagnosis of post-surgical fine-needle aspiration biopsies of thyroid lesions with indeterminate cytology using HRMAS NMR-based metabolomics. *Metabolomics*, *14*(10), 141. https://doi.org/10.1007/s11306-018-1437-6

Rondon, L. J., Farges, M. C., Davin, N., Sion, B., Privat, A. M., Vasson, M. P., … Courteix, C. (2018). L-Arginine supplementation prevents allodynia and hyperalgesia in painful diabetic neuropathic rats by normalizing plasma nitric oxide concentration and increasing plasma agmatine concentration. *European Journal of Nutrition*, *57*(7), 2353–2363. https://doi.org/10.1007/s00394-017-1508-x

Schroecksnadel, K., Winkler, C., Duftner, C., Wirleitner, B., Schirmer, M., & Fuchs, D. (2006). Tryptophan degradation increases with stage in patients with rheumatoid arthritis. *Clinical Rheumatology*, *25*(3), 334–337. https://doi.org/10.1007/s10067-005-0056-6

Sethi, G., Sung, B., & Aggarwal, B. B. (2008). Nuclear factor-kappaB activation: From bench to bedside. *Experimental Biology and Medicine (Maywood, N.J.)*, *233*(1), 21–31.

Shell, W. E., Pavlik, S., Roth, B., Silver, M., Breitstein, M. L., May, L., & Silver, D. (2016). Reduction in pain and inflammation associated with chronic low back pain with the use of the medical food Theramine. *American Journal of Therapeutics*, *23*, e1353–e1362. https://doi.org/10.1097/MJT.0000000000000068

Tsuji, H., Tetsunaga, T., Tetsunaga, T., Nishida, K., Misawa, H., & Ozaki, T. (2019). The factors driving self-efficacy in intractable chronic pain patients: A retrospective study. *Journal of Orthopaedic Surgery and Research*, *14*(1), 473. https://doi.org/10.1186/s13018-019-1535-9

Valenzuela, R., & Videla, L. A. (2020). Impact of the co-administration of N-3 fatty acids and olive oil components in preclinical nonalcoholic fatty liver disease models: A mechanistic view. *Nutrients*, *12*(2). https://doi.org/10.3390/nu12020499

Wang, W., Zhang, J., Wang, H., Wang, X., & Liu, S. (2019). Vitamin D deficiency enhances insulin resistance by promoting inflammation in type 2 diabetes. *International Journal of Clinical and Experimental Pathology*, *12*(5), 1859–1867.

Wang, Y., Bi, C., Pang, W., Liu, Y., Yuan, Y., Zhao, H., … Li, Y. (2019). Plasma metabolic profiling analysis of gout party on acute gout arthritis rats based on UHPLC–Q-TOF/MS combined with multivariate statistical analysis. *International Journal of Molecular Sciences*, *20*(22). https://doi.org/10.3390/ijms20225753

Yang, Q. J., Zhao, J. R., Hao, J., Li, B., Huo, Y., Han, Y. L., … Guo, C. (2018). Serum and urine metabolomics study reveals a distinct diagnostic model for cancer cachexia. *Journal of Cachexia, Sarcopenia and Muscle*, *9*(1), 71–85. https://doi.org/10.1002/jcsm.12246

Zhang, L., Wei, T. T., Li, Y., Li, J., Fan, Y., Huang, F. Q., … Qi, L. W. (2018). Functional metabolomics characterizes a key role for *N*-acetylneuraminic acid in coronary artery diseases. *Circulation*, *137*(13), 1374–1390. https://doi.org/10.1161/CIRCULATIONAHA.117.031139

Zhao, Z., Hiraoka, Y., Ogawa, H., & Tanaka, K. (2018). Region-specific deletions of the glutamate transporter GLT1 differentially affect nerve injury-induced neuropathic pain in mice. *Glia*, *66*, 1988–1998.

Zhou, P., Zhou, N., Shao, L., Li, J., Liu, S., Meng, X., … Wu, A. (2018). Diagnosis of *Clostridium difficile* infection using an UPLC–MS based metabolomics method. *Metabolomics*, *14*(8), 102. https://doi.org/10.1007/s11306-018-1397-x

How to cite this article: Zhang W, Lyu J, Xu J, et al. The related mechanism of complete Freund's adjuvant-induced chronic inflammation pain based on metabolomics analysis. *Biomedical Chromatography*. 2021;35:e5020. https://doi.org/10.1002/bmc.5020